Computed tomography scanning with simultaneous patient translation

Carl R. Crawford and Kevin F. King
GE Medical Systems, Milwaukee, Wisconsin 53201

(Received 27 November 1989; accepted for publication 14 March 1990)

This paper deals with methods of reducing the total time required to acquire the projection data for a set of contiguous computed tomography (CT) images. Normally during the acquisition of a set of slices, the patient is held stationary during data collection and translated to the next axial location during an interscan delay. We demonstrate using computer simulations and scans of volunteers on a modified scanner how acceptable image quality is achieved if the patient translation time is overlapped with data acquisition. If the concurrent patient translation is ignored, structured artifacts significantly degrade resulting reconstructions. We present a number of weighting schemes for use with the conventional convolution/backprojection algorithm to reduce the structured artifacts through the use of projection modulation using the data from individual and multiple slices. We compare the methods with respect to structured artifacts, noise, resolution and to patient motion. Review of preliminary results by a panel of radiologists indicates that the residual image degradation is tolerable for selected applications when it is critical to acquire more slices in a patient breathing cycle than is possible with conventional scanning.

Key words: computed tomography, helical scanning, spiral scanning

I. INTRODUCTION

Computed tomography (CT) scanners are designed to perform what we denote *studies* of a patient. The result of a study is a set of images of contiguous axial slices. Most clinical CT scanners collect the data necessary to reconstruct the slices using a repetitive four-step process. In the first step a source/detector combination, mounted on a gantry, is accelerated to a constant rotation speed. Second, for approximately 360° of rotation, the source is enabled and the readings, called projections or views, are measured by the detector. The gantry rotates in the xy plane of a Cartesian coordinate system which is also known as the slice plane. In the third step the source/detector combination is decelerated to a rest position. Finally, in the fourth step the table, on which the patient lies, is indexed so that the patient is at the location of the next axial slice. The table moves along the z axis which is perpendicular to the xy plane. The total time that it takes to perform steps one, three and four is denoted the interscan delay (ISD). It should be noted that step four can be overlapped with steps one and three. The process is repeated until all the slices in a study are collected. We denote this type of scanning *constant z axis* (CZA). Figure 1 shows the relative positions of the gantry and the patient for CZA.

Collimators are placed in the path between the source and detector in order to define an approximate slab, denoted the slice volume, in which projection measurements are acquired. The slice profile is defined to be the response to small objects at various displacements parallel to the z-axis.[1] In general, the slice profile is a function of the radial distance from the isocenter of the scanner. The slice width or thickness is usually defined to be the full width at half-maximum (FWHM) of the slice profile at the isocenter.

CT scans of the body are usually acquired in groups while respiration is suspended. An ISD is required between each pair of slices in a group. After these slices are acquired, the scanner waits a time called the intergroup delay (IGD) before beginning the next group of scans. The patient is allowed to breathe during the IGD. We define the scan rate of a scanner to be the ratio of the number of scans per group to the sum of the time required to collect the slices plus the IGD.

As the resolving power of CT methods increases, additional slices are required in the z dimension. The time and expense of a tomographic study increases with the number of slices required. Also, longer study times increase the discomfort to the patient who must remain nearly motionless to preserve the fidelity of the tomographic reconstructions. Shorter study times can increase the enhancement caused by contrast agents or may reduce the dose of the agent for a given level of enhancement. Accordingly, there is considerable interest in increasing the scan rate. The rate can be increased by reducing the time it takes for any of the four steps listed above assuming a fixed breath-holding time and IGD. In this paper we concentrate on methods to eliminate the ISD. We make the assumption that data acquisition is not limited by tube cooling or by bandwidth limitations in accessing and storing the projection data.

The gantry is accelerated and decelerated because of the finite length of the cables that are used to interface to components that rotate. We make the assumption that the scanner can rotate continuously and scans can start at any angle and therefore the acceleration and deceleration times of steps one and three can be eliminated. Techniques for constructing a continuously rotating scanner have been described elsewhere.[2,3]

The mathematics of tomographic reconstruction assumes

 0094-2405/90/060967-16$01.20

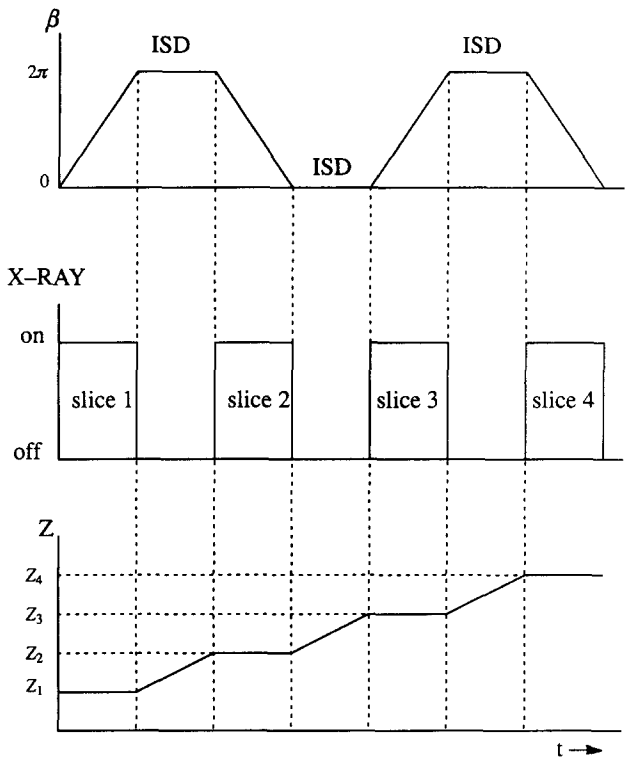

FIG. 1. Schematic diagram for constant z-axis scanning (CZA). β is the gantry rotational angle, t is time, z is the table location, and ISD is the interscan delay.

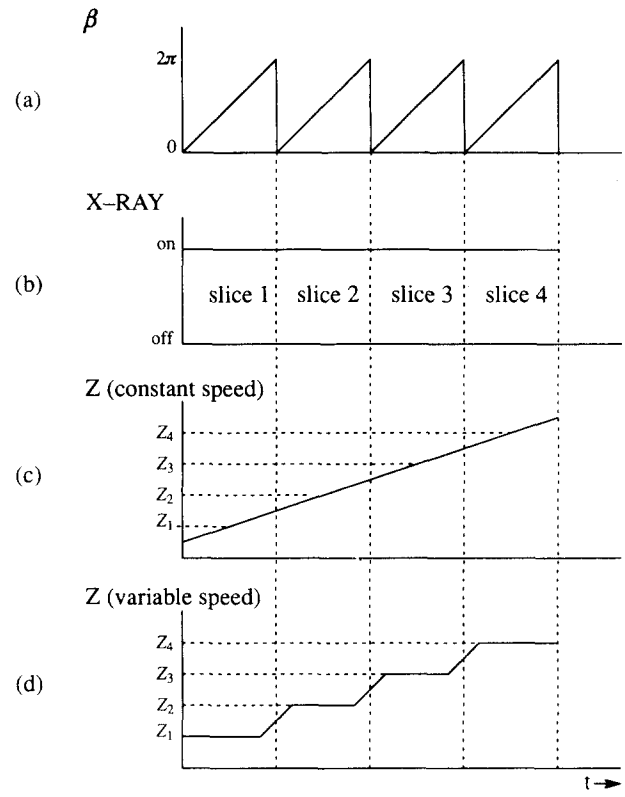

FIG. 2. Schematic diagram for constant speed helical scanning (CSH) and for variable speed helical scanning (VSH). The gantry rotational angle β is shown in (a) and the state of the x-ray source is shown in (b). The table location z is shown for CSH in (c) and for VSH in (d). In this figure, t indicates time.

that a consistent projection set is acquired. Consistency means that the projections are collected within the same plane through the object. This condition implies that the patient should remain stationary during data collection. The projection data obtained with CZA is approximately consistent if compensation is made for physical effects such as system nonlinearities,[4-6] beam hardening,[7-9] partial volume,[10,11] and scatter.[12,13] Note that partial volume artifacts are usually in the form of streaks between objects that partially protrude into the slice volume and a degradation of the slice profile.

It follows from the mathematics that the only way to reduce the ISD is by increasing the speed at which the patient is indexed. However, if the patient is indexed too quickly, the resulting acceleration forces could induce motion which in turn would degrade image quality[14,15] or cause motion sickness. Another way that the ISD due to patient repositioning between slices can be eliminated is if the translation is overlapped with data acquisition. Data collection in this scheme generates inconsistent projections because the patient is moving during data acquisition. Artifacts are introduced because of this deviation if there is any significant change in the object along the z axis. The purpose of this paper is to show how the inconsistencies affect image quality. Typically, the artifacts appear as streaks, in the direction of the first and last views, emanating from the edges of objects which change significantly during a scan. We also show methods to correct for the inconsistencies.

Consider the case when the patient is moved at a constant speed during data acquisition as shown in Fig. 2. This type of scanning is termed *helical scanning* and refers to the apparent path of a point on the gantry with respect to a reference point on the patient. As used in this paper, *constant speed helical* (CSH) shall refer to the use of constant speed translation of the patient during the acquisition of projection data. We define the pitch of a helical scan to be the ratio of the distance that the table moves during 360° of gantry rotation to the slice thickness that would be obtained if the table did not move. A helical scan with a pitch of zero is equivalent to CZA.

Several methods have been introduced to reduce the artifacts caused by CSH. Mori[16] suggested that the pitch of the helical scan be reduced and then to average the projection data corresponding to consecutive 360° projection sets. The effect is equivalent to using a larger slice thickness and to move less in the z direction during the rotation of the gantry. Artifacts are reduced using this method, but at the expense of additional scanning time necessitated by the lower scanning pitch. This method reduces, to some extent, the advantages in scan rate to be gained with helical scanning. Mori also indicated that additional artifact suppression may be

gained by changing the weighting of the first and last projections of the consecutive sets in the *averaging* process to give greater weight to the projections closest to the slice plane.

Nishimura and Miyazaki[17] proposed a second approach to reduce the errors caused by CSH. Two sets of 360° of projections are linearly interpolated so that one set is generated at a constant z location. (We would like to refer the reader to three recently published abstracts that appear to describe the same method.[18–20]) We demonstrate that their method significantly increases the slice profile degradation caused by partial volume relative to CZA. Because of the increase in artifacts, Nishimura's method is approximately equivalent to using CZA with a larger slice thickness.

We present a number of new weighting schemes that eliminate the errors caused by CSH. One type of weighting is derived so that a consistent halfscan[21] is formed. Another type of weighting is obtained by noting that the artifacts generated with helical scanning are similar to motion artifacts. We found that an extant motion correction algorithm[22] is effective in removing the artifacts caused by helical scanning. The weighting schemes utilize projection sets acquired with gantry rotation $< 720°$. The degradation of the slice profile is reduced because of the decrease in gantry rotation.

We also present a second method to move the table during simultaneous data acquisition. With this method, the patient is translated at a variable speed as shown in Fig. 2. We call this method *variable speed helical* (VSH). The method causes a concentration of stationary projection data at the slice plane. The data are reconstructed by attenuating the projections at the ends of the set, where the table is moving, and to emphasize the projections in the middle, where the table is stationary. We show that VSH produces slightly more structured artifacts than the best CSH algorithm. However, the slice profile degradation can be significantly less than that obtained with CSH.

In the next section, we develop the data-acquisition schemes and the reconstruction algorithms for CSH and VSH. We then present the results of a computer simulation study that was undertaken to measure the relative performance of the various helical scanning methods. Then we present the results of an experiment in which we scanned volunteers on a modified scanner. Finally, we present a discussion of the anticipated clinical utility of helical scanning and the impact of helical scanning on scan rate.

II. DATA ACQUISITION AND RECONSTRUCTION

In this section we discuss a number of algorithms that remove the artifacts that would be generated if helically acquired data were reconstructed without correction. We address correction methods for both CSH and VSH. All the correction methods begin by selecting a length of projection data and choosing a set of weights that reduce the inconsistencies caused by table motion.

A. CSH data acquisition

For the following discussion we focus our attention on the third generation geometry.[23] The results can be extended to fourth generation[24] and fan-parallel geometry.[25] The geometry of third generation scanning is shown in Fig. 3. The view and detector angles are denoted β and γ, respectively. The maximum detector angle is γ_m. All angles are positive as defined in Fig. 3. The direction normal to the scan plane is denoted z. We denote the traditional fanbeam reconstruction algorithm with 2π views without special weighting in the reconstruction[26] *fullscan*. The abbreviation FS denotes the use of fullscan.

Let $P(\beta,\gamma,z)$ denote a projection acquired at view and detector angles β and γ, respectively, and at table position z. For this discussion, we ignore the slice thickness and other physical effects. In CZA acquisition, z is an independent variable since $P(\beta,\gamma,z)$ is acquired with the table stationary at various values of z for β in the range $(0,2\pi)$ and γ in the range $(-\gamma_m,\gamma_m)$. In CSH, z is not an independent variable since we acquire $P(\beta,\gamma,z)$ at z locations linearly related to the view angle β so that $z(\beta,\gamma) = c\beta$, where c is a constant.

If CSH data are reconstructed without compensation for the table motion (the reconstruction is denoted CSH-FS), structured artifacts result because the projection data are inconsistent, as is demonstrated later. Our goal is to develop compensation algorithms which reduce the artifacts to an acceptable level. We derive two types of compensation methods. The first type employs interpolation and extrapolation to create a consistent data set effectively acquired at a constant z location from the projection data. The second compensation type involves the realization that the table motion causes certain portions of the data to be inconsistent when, instead, they should be nearly identical,for example at 0° and 360°. This latter compensation involves blending the "seams" of the data in these areas of greatest inconsistency.

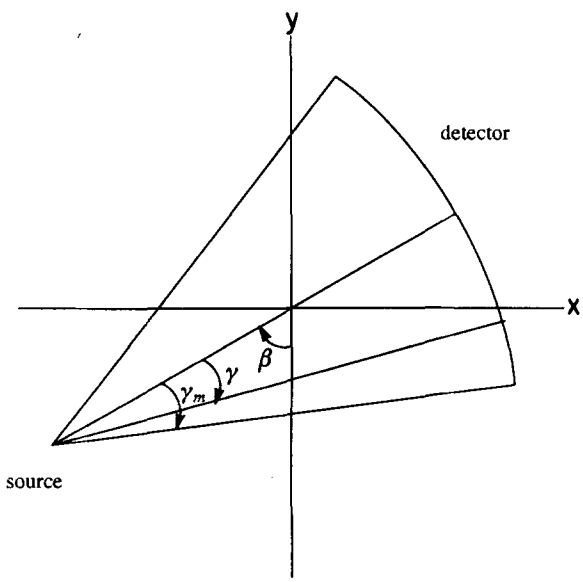

FIG. 3. The geometry of a third generation scanner. The view and detector angles are denoted β and γ, respectively. The maximum detector angle is γ_m. All angles are positive as shown.

B. CSH fullscan with interpolation

In the CSH fullscan method, moving data is acquired for β in the range $(0,4\pi)$. A set of CZA data for β in the range $(0,2\pi)$ is approximated by linear interpolation of data on opposite sides of the slice plane located at the position corresponding to view $\beta_{sp} = 2\pi$.

We wish to obtain the projection $P(\beta_1,\gamma_1,z_{sp})$ which would result from stationary scanning at table position z_{sp}. Using linear interpolation

$$P(\beta_1,\gamma_1,z_{sp}) = w_1 P(\beta_1,\gamma_1,z_1) + w_2 P(\beta_2\gamma_2 z_2) \quad (1)$$

where

$$\beta_2 = \beta_1 + 2\pi$$

$$\gamma_2 = \gamma_1. \quad (2)$$

The interpolation weights w_1 and w_2 are given by

$$w_1 = \frac{\beta_2 - \beta_{sp}}{\beta_2 - \beta_1}$$

$$w_2 = \frac{\beta_{sp} - \beta_1}{\beta_2 - \beta_1} \quad (3)$$

One possible reconstruction method is to perform the interpolation in Eq. (1) prior to filtered backprojection, producing a data set with $z = z_{sp}$ and β in the interval $(0,2\pi)$. Since filtered backprojection is linear, an alternative is to multiply the data by interpolation weights $w(\beta,\gamma)$ and perform filtered backprojection on the entire $(0,4\pi)$ data set. We prefer the latter method which, from now on, we assume for all algorithms, since it enables pipelining the reconstruction process. The weights $w(\beta,\gamma)$ for this method are

$$w(\beta,\gamma) = \begin{cases} \dfrac{\beta}{2\pi} & 0 \leqslant \beta \leqslant 2\pi \\ \dfrac{4\pi - \beta}{2\pi} & 2\pi \leqslant \beta \leqslant 4\pi \end{cases} \quad (4)$$

The weights are continuous everywhere, go to zero at $\beta = 0$ and $\beta = 4\pi$, and go to one at $\beta = 2\pi$. We use the abbreviation CSH-HI to denote this algorithm which was also proposed by Nishimura and Miyazaki.[17]

C. CSH halfscan with interpolation

Reconstruction with less than 4π views can be achieved by using the redundancy of fanbeam data as with a conventional halfscan reconstruction (see Appendix C). In this method, moving data is acquired for β in the range $(0,2\pi + 4\gamma_m)$. Stationary data for β in the range $(0,\pi + 2\gamma_m)$ is approximated by linear interpolation of data on *opposite* sides of the slice plane located at the position corresponding to $\beta_{sp} = \pi + 2\gamma_m$. The advantage of this method over the previous method, CSH-HI, is that this method uses fewer views and therefore has less table and patient motion during the scan. As is seen later, greater table motion causes the reconstructed image to have a greater effective slice width.

A description of the reconstruction weights is given with reference to Fig. 4 showing the Radon space (β vs γ) for the acquired data. We define redundant data as data acquired along geometric rays which would be identical in the absence of patient motion. The redundant data are acquired from both parallel and antiparallel directions. In this figure, areas of redundant data are similarly striped. The letters A through D show the boundaries of these regions. The linear interpolation for each region must correctly combine it with another similarly striped area on the opposite side of the reconstruction slice plane at $\beta_{sp} = \pi + 2\gamma_m$.

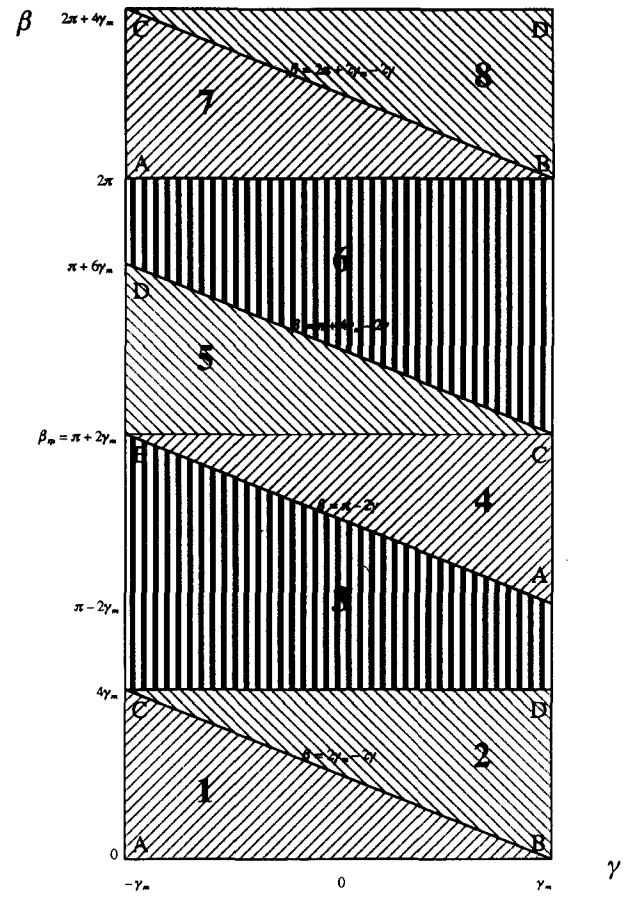

FIG. 4. Radon space for the data acquired with the CSH-HH algorithm. The slice plane is crossed at $\beta = \pi + 2\gamma_m$. Areas of redundant data are similarly striped.

The data from regions 1 through 4 form a complete set of halfscan data in the absence of motion. The combination of the similarly striped areas can be thought of as creating a new set of stationary halfscan data in regions 1 through 4. We denote the stationary data thus created in these regions with the notation 1* through 4*.

Region 1 must be combined with region 7 to effectively create stationary data for region 1*. Region 1 is not combined with region 4 (assuming we avoid extrapolation) since 4 and 1 are on the same side of the slice plane. Similarly, region 3 is combined with region 6. Region 2 however, could be combined with either region 5 or region 8 since both are on opposite sides of the slice plane. If both combinations were used, region 2* would effectively be generated twice. The two versions would be nearly identical, so that shading

would result if both were used and duplicates of the other regions were not used. We assign two sets of linear interpolation weights to region 2, one for combining with region 5, the other for combining with region 8. The redundancy is then controlled by a separate set of blending weights (called half scan weights). Continuing the discussion, region 4 is combined with region 7 to effectively create stationary data for region 4*. Since region 7 must also be combined with region 1, it requires two sets of weights. Since region 4 is redundant with region 1, if the table is stationary, this redundancy must also be eliminated according to the previous discussion.

By this logic we arrive at the following weighting scheme. Regions 1, 3, 4, 5, 6, and 8 have one linear interpolation weight to correct for table motion. Regions 2 and 7 have two. The linear interpolation weights (called helical weights) are denoted $he_i(\beta,\gamma)$ or $he'_i(\beta,\gamma)$ where i is the region number. Each interpolation weight is accompanied by a halfscan weight to suppress redundancy in the combined stationary data. The halfscan weights are denoted $ha_i(\beta,\gamma)$ or $ha'_i(\beta,\gamma)$. The combined weights for each region are

$$\begin{aligned}
&1: he_1(\beta,\gamma)ha_1(\beta,\gamma)\\
&2: he_2(\beta,\gamma)ha_2(\beta,\gamma) + he'_2(\beta,\gamma)ha'_2(\beta,\gamma)\\
&3: he_3(\beta,\gamma)ha_3(\beta,\gamma)\\
&4: he_4(\beta,\gamma)ha_4(\beta,\gamma)\\
&5: he_5(\beta,\gamma)ha_5(\beta,\gamma)\\
&6: he_6(\beta,\gamma)ha_6(\beta,\gamma)\\
&7: he_7(\beta,\gamma)ha_7(\beta,\gamma) + he'_7(\beta,\gamma)ha'_7(\beta,\gamma)\\
&8: he_8(\beta,\gamma)ha_8(\beta,\gamma).
\end{aligned} \tag{5}$$

The helical weights are dictated by the choice of linear interpolation and the assumption of which data regions are to be combined. We use the convention that one realization of region 2* is from $he_2(\beta,\gamma)ha_2(\beta,\gamma)$ and $he_8(\beta,\gamma)\times ha_8(\beta,\gamma)$ and that the other is from $he'_2(\beta,\gamma)ha'_2(\beta,\gamma)$ and $he_5(\beta,\gamma)ha_5(\beta,\gamma)$. Similarly, region 1* results from $he_1(\beta,\gamma)ha_1(\beta,\gamma)$ and $he_7(\beta,\gamma)ha_7(\beta,\gamma)$ while region 4* results from $he_4(\beta,\gamma)ha_4(\beta,\gamma)$ and $he'_7(\beta,\gamma)ha'_7(\beta,\gamma)$. With this convention the helical weights are given by

$$he_1(\beta,\gamma) = he_2(\beta,\gamma) = \frac{\pi+\beta-2\gamma_m}{2\pi}, \tag{6}$$

$$he'_2(\beta,\gamma) = he_3(\beta,\gamma) = he_4(\beta,\gamma) = \frac{\beta+2\gamma-2\gamma_m}{\pi+2\gamma}, \tag{7}$$

$$he_5(\beta,\gamma) = he_6(\beta,\gamma) = he'_7(\beta,\gamma) = \frac{2\pi-\beta-2\gamma+2\gamma_m}{\pi-2\gamma}, \tag{8}$$

$$he_7(\beta,\gamma) = he_8(\beta,\gamma) = \frac{3\pi-\beta+2\gamma_m}{2\pi}. \tag{9}$$

If we were to set all of the halfscan weights equal to one in Eq. (5), region 2* would be created twice and regions 1*, 3*, and 4* would be created once. Regions 1* and 4* are also redundant. The halfscan weights could be chosen in a variety of ways to suppress the redundant data. One way is to suppress the creating of region 1* and one of the versions of region 2*. Creation of region 1* arises from regions 1 and 7. Creation of region 2* arises from regions 2 and 8 as well as 2 and 5. Suppose we suppress the version of region 2* created from regions 2 and 8. The halfscan weights are

$$ha_1(\beta,\gamma) = ha_2(\beta,\gamma) = ha_7(\beta,\gamma) = ha_8(\beta,\gamma) = 0 \tag{10}$$

$$ha'_2(\beta,\gamma) = ha_3(\beta,\gamma) = ha_4(\beta,\gamma) = ha_5(\beta,\gamma) = ha_6(\beta,\gamma) = ha'_7(\beta,\gamma) = 1. \tag{11}$$

Triangles 1 and 8 receive zero weighting. Note that the weights for this case suppress data combinations which have the greatest temporal separation, namely 1 and 7 and 2 and 8. A desirable feature of the combined weights in this case is that they are continuous everywhere.

Many other ways of suppressing the redundant data are possible. For example, the two versions of region 2* could be averaged and also regions 1 and 4 could be averaged. In this case, $ha_i(\beta,\gamma)$ would be 1 for regions 3 and 6 and all other halfscan weights would be 0.5.

We use the abbreviation CSH-HH to denote the algorithms described in this section. In the computer simulations and experimental data collection that are presented later, the weights described in Eq. (10) and Eq. (11) are used.

D. CSH halfscan with extrapolation

In this method, moving data is acquired for β in the range $(0,2\pi)$. CZA data for β in the range $(0,\pi+2\gamma_m)$ is approximated by linear interpolation and extrapolation of data on *either* side of the slice plane located at the position corresponding to $\beta_{sp}=\pi$. The extrapolation derives from the situation where data on the *same* side of the slice plane are effectively combined. In contrast, in CSH-HH, data on *opposite* sides of the slice plane are combined. Figure 5 shows the Radon space for the acquired data. Boundaries of redundant data are marked with the letters A through E. For data such

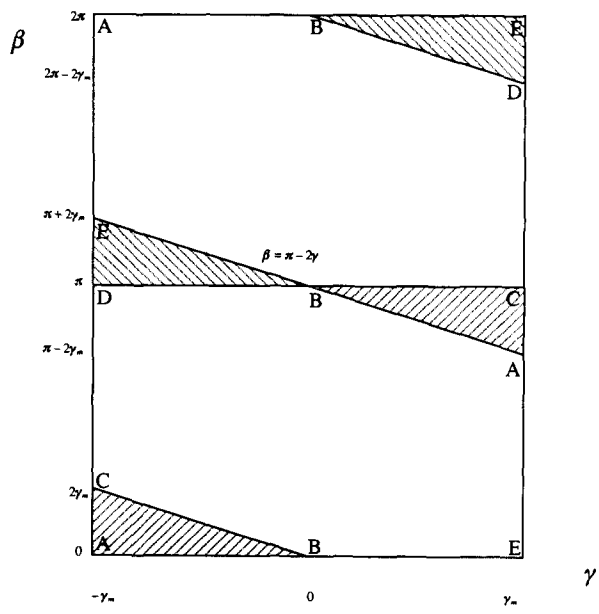

FIG. 5. Radon space for the data acquired with the CSH-HE algorithm. The shaded areas are extrapolated whereas the unshaded areas are interpolated.

as that in the shaded triangle ABC, the redundant data is on the same side of the slice plane at $\beta_{sp} = \pi$. Similar comments hold for the other shaded triangle BDE. These shaded areas are extrapolated whereas the unshaded areas are interpolated.

Originally, we derived the interpolative method, CSH-HH, because we were concerned about the effects of extrapolation and intuitively felt that interpolation should be better. As shown later, however, there is no degradation caused by extrapolation. The advantage of this method over CSH-HH is that this method uses fewer views and therefore has less table motion and patient motion within the scan. Reducing the table motion reduces the effective width of the reconstructed slice as is seen later.

The interpolation weights are given by Eq. (3) and the view data to be combined is related by

$$\begin{aligned} \beta_2 &= \beta_1 + \pi + 2\gamma_1 \\ \gamma_2 &= -\gamma_1, \end{aligned} \tag{12}$$

giving

$$w(\beta,\gamma) = \begin{cases} \dfrac{\beta + 2\gamma}{\pi + 2\gamma} & 0 \leqslant \beta \leqslant \pi - 2\gamma \\ \dfrac{2\pi - \beta - 2\gamma}{\pi - 2\gamma} & \pi - 2\gamma \leqslant \beta \leqslant 2\pi \end{cases} \tag{13}$$

Note that $w(\beta,\gamma)$ is discontinuous in γ along the line $\beta = \pi - 2\gamma$, except at $\gamma = 0$. Data along this line are equivalent to data along the lines $\beta = 0$ and $\beta = 2\pi$ according to Eq. (12). Since $w(\beta,\gamma)$ is continuous in γ along these latter lines, there is an inconsistency in the discretely sampled weighted projection data leading to streaks which appear to originate from the first view and become deeper for greater distances away from isocenter. The discontinuity can be eliminated by feathering $w(\beta,\gamma)$ across the line $\beta = \pi - 2\gamma$ as discussed in Appendix D. A feathering distance of 10 channels has been found sufficient. We use the abbreviation CSH-HE to denote this algorithm.

E. CSH underscan and overscan

A key effect of the table motion is a large discontinuity between data at $\beta = 0$ and $\beta = 2\pi$. We therefore decided to apply motion correction algorithms which have been tailored to correct for similar discontinuities due to patient motion. Underscan and overscan (see Appendices A and B) are two such algorithms. Although the data discontinuity due to table motion is much larger than that due to patient motion, we found that the algorithms still worked. They are similar to the interpolation methods discussed above in the sense that they reduce the inconsistency of the data set by underweighting the data near the beginning and end of the scan. They differ in the sense that they do not create a set of views corresponding to data acquired at a constant table location. Underscan and overscan have the advantage relative to CSH-HI of requiring less than 4π views of data. Overscan has the disadvantage relative to underscan of requiring more than 2π views of data. We use the abbreviations CSH-OS and CSH-US to denote the use of overscan and underscan, respectively, with CSH.

F. CSH halfscan

Halfscan algorithms underweight some of the redundant data at the beginning and end of the scan (see Appendix C). Such algorithms reduce the data inconsistency caused by table motion and could be expected to afford some artifact reduction. They do not create a data set acquired at a constant table position. Halfscan requires the least amount of data of any of the reconstruction methods discussed, namely $\pi + 2\gamma_m$ views, with the advantage that the table does not move as far during the scan. We use the abbreviation CSH-HS to denote the use of halfscan with CSH.

G. Generalized CSH data acquisition and reconstruction

Fanbeam projections can be mapped into parallel projections using a technique called rebinning or fan parallel.[25] The resulting parallel projections are reconstructed using the filtered backprojection algorithm for parallel projections.[27] The table position is not constant for the rebinned parallel views. The above algorithms can be extended to handle this case.

In fourth generation geometry, it is conventional to rebin the scan data into detector-vertex fans, i.e., groups of rays emanating from the same detector and acquired at a range of tube positions.[24] These detector fans are analogous to third generation data fans except that, in fourth generation geometry, the tube and detector are interchanged relative to third generation. Since the table motion is synchronized with the tube motion, the table position is not constant over one rebinned fanbeam view. The above algorithms can be extended to handle this case as well.

When the algorithms are extended to the case of rebinned or fourth generation projections, weights that were continuous in the third generation case will be discontinuous in the former cases. We have found that the feathering algorithm, which is presented in Appendix D, can be applied to remove the discontinuities without having an impact on image quality.

The interpolative methods that we presented earlier in this section were based on linear interpolation. We found through computer simulation that higher-order Lagrange interpolation was inferior to linear interpolation. Skrabacz[28] and Bresler and Skrabacz[29] recently developed helical scanning interpolators based on optimization criteria that were used for the recovery of band-limited functions.[30,31] Their interpolator is optimized to minimize the maximum normalized differential error in the resulting reconstructions. They applied their interpolator to the case of at least 720° of parallel projections. Based on their work, we can extend their algorithm to the interpolation of at least 1440° of fanbeam projections. The coefficients for the resulting interpolation can be found by solving the following set of linear equations

$$\operatorname{sinc}\left[\alpha\pi\left(k + \frac{\beta}{2\pi}\right)\right] = \sum_{m=-L+1}^{L} a_\beta(m)\operatorname{sinc}[\alpha\pi(m-k)],$$

$$k = -L+1, \cdots, L \tag{14}$$

where $\text{sinc}(x) = \frac{\sin(x)}{x}$, a_β are the view dependent interpolation coefficients, the order of the interpolator L must be greater than or equal to two, and α is a design parameter which is in the range [0,1]. It is seen that the length of the interpolator is $2L$. As α approaches zero, the interpolator reduces to a two-point linear interpolator for the case of $L = 2$.

H. VSH data acquisition and reconstruction

In VSH acquisition, data are acquired with β in the range $(0,2\pi)$. The table is stationary for most of the scan and translates between slice positions at the beginning and end of the scan as shown in Fig. 2. We use the abbreviations VSH-FS to denote VSH acquisition without projection weighting.

We examined the use of underscan and halfscan to perform the reconstruction. It is interesting to note that, with a sufficiently brief table motion, and appropriate choice of the halfscan start angle, the table is stationary for all reconstructed data, reducing to the CZA case. We did not pursue the use of halfscan with VSH because of its reduction to CZA.

For the underscan case, the reconstruction can be somewhat optimized by choosing the underscan angle to match the duration of table motion at the beginning and end of each slice. We use the abbreviation VSH-US to denote the use of underscan with VSH. Since our primary interest is third generation geometry, we did not pursue VSH with fan-parallel or fourth generation geometry to any extent.

I. Summary

In this section we have presented a number of different methods for collecting and reconstructing helical data. In the next two sections we compare the methods using computer simulations and experimental data. The last section of the paper addresses the issue of the optimum method. The comparisons are made with respect to CZA reconstructions. We also show the images that result if the table motion is ignored and the data are reconstructed using the fullscan algorithm. In order to make the comparisons easier, Table I contains a summary of the methods presented above.

TABLE I. Summary of the data acquisition and reconstruction algorithms discussed in Sec. II. The maximum detector angle in a fanbeam projection is γ_m and β_o is the overscan angle.

Method	Translation	Projections	Projection Weighting
CZA-FS	none	2π	none
CSH-FS	constant	2π	none
CSH-HS	constant	$\pi + 2\gamma_m$	halfscan
CSH-OS	constant	$2\pi + \beta_o$	overscan
CSH-US	constant	2π	underscan
CSH-HI	constant	4π	interpolation
CSH-HH	constant	$2\pi + 4\gamma_m$	interpolation & halfscan
CSH-HE	constant	2π	extrapolation
VSH-FS	variable	2π	none
VSH-US	variable	2π	underscan

III. COMPUTER SIMULATIONS

In this section we present the results of computer simulations that were used to study the image quality that results with CSH and VSH. The areas of interest are the slice profiles, level of artifact suppression and the signal-to-noise ratio.

A. Details of simulation

A program was written to generate line integrals through a field of ellipsoids. The source-to-center distance, source-to-detector distance and detector spacing were 630, 1100, and 1 mm, respectively. A focal spot was simulated which was 0.7 by 0.9 mm (axial by width). A target angle of 90° was used. The incorporation of a realistic target angle would cause some loss of resolution at the perimeter of the scanner.[32] In the discussion of the results presented below, all comparisons are made relative to the CZA scan at the same place in the field-of-view. Therefore, the degenerate target angle should not affect the comparison of the algorithms.

The focal spot and the detector are broken up into a number of elements called *source-lets* and *detector-lets*, respectively. We used 5 by 1 and 12 by 5 for the source and detector, respectively, where the notation is the number of axial positions by the number of azimuthal positions. A number of simulations were run to verify that the number of *lets* was sufficient to model the two-dimensional integrals over the two apertures. No source-lets were used in the azimuthal direction because we were primarily interested in slice profiles and not in spatial resolution. The simulated source starts at the top of the vertical axis.

The number of projections that were generated for each 360° of gantry rotation was 200. The low number of projections caused some streak artifacts[33] to be present in the resulting images. Since conclusions are made using comparable images, the low number is not a problem. Quarter-detector offset[34] was not utilized and therefore some aliasing[35] was present in the results. However, the aliasing artifacts were minor compared to artifacts caused by helical scanning.

The slice thickness was determined by changing the length of the detector along the z axis instead of using collimation. Calculations showed that the slice profile at the isocenter was slightly smaller than when collimators were used. Off-center, the slices were slightly larger. We do not feel that these differences had a significant effect on the results since comparisons are made relative to CZA. A 10-mm slice thickness was simulated. When helical data were generated, the simulated table was translated 10 mm during each 360° of gantry rotation corresponding to a unity pitch.

When VSH was simulated, a parameter called *vbreak* was introduced which is the fractional number of views that are affected at the beginning and at the end of the scan. The program translated the table five millimeters at the beginning and end of the scan during the acquisition of a number of views equal to vbreak times the total number of views. The table is translated using a piecewise constant velocity profile for each view as shown in Fig. 2. In practice, a nonlinear

profile would be implemented. We believe that the constant profile is acceptable for the simulations.

When underscan and overscan reconstructions were made, the underscan and overscan angles were set to 45°.

B. Simulation of slice profile

In order to measure the slice profile, we simulated a wire using a very long and narrow ellipsoid which is tilted 45° with respect to the slice plane. The reconstruction shows the intersection of the ellipsoid with the slice, and the length of the intersection is taken as a measure of slice profile. The ellipsoid was 600 mm long and had a 1-mm diam cross section at its center. The center of the ellipsoid was positioned at the isocenter.

Figure 6 shows the reconstructions of the wire for different data collection and reconstruction modes. The gray scale has been expanded in order to display subtle artifacts. A number of artifacts are seen along with cross sections of varying lengths. The strong streaks are vertical because the tube starts at the top of the simulated scanner. There are little black and white regions around the cross sections due to inconsistencies in the projection data as a direct result of the helical scanning.

The slice profiles can be obtained by projecting the maximum values of the images onto the horizontal axis. The results are presented in Fig. 7. Helical scanning changes the fairly square profile of CZA into a triangularly shaped profile. The FWHM values for the simulations are summarized in Table II. Because the profiles for CSH and VSH are not generally rectangular, we also give the values of the full width at tenth-maximum (FWTM). We suspect that the FWHM and FWTM are not necessarily meaningful measures of the effective slice width because of the irregular slice profiles. We present the measures because they are traditionally used.

Among the CSH methods, CSH-HS shows the smallest FWTM and the most rectangular slice profile (see Fig. 7). As seen in the next section, CSH-HS has much poorer signal-to-noise than any of the methods and might therefore be objectionable. Still considering only CSH methods, CSH-HE and CSH-HH have the next smallest FWTM. However, CSH-HE might be preferable to CSH-HH because of its smaller FWHM. Only slightly worse than CSH-HE is CSH-US. Finally, CSH-OS and CSH-HI have significantly larger values of FWTM and FWHM.

Comparing VSH and CSH methods, Fig. 7 shows that VSH has a more rectangular profile than all CSH methods except CSH-HS for values of vbreak less than 0.3. In fact the VSH FWTM is better than all CSH cases for vbreak less than 0.2. The VSH case with vbreak equal to 0.1 is almost equivalent to CZA.

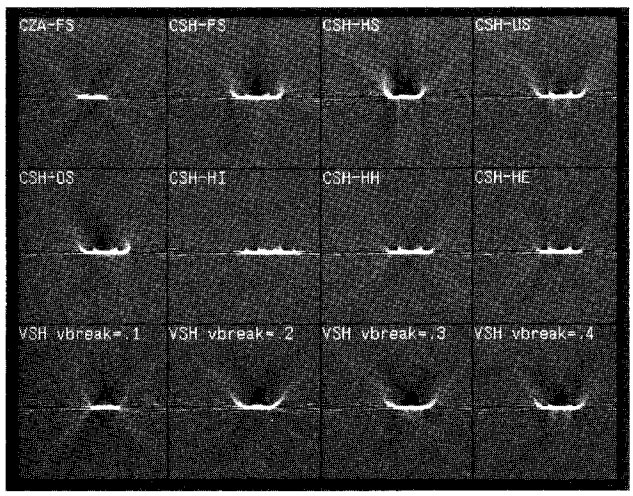

FIG. 6. Simulated reconstructions of a tilted wire for different data collection and reconstruction modes. A 10-mm slice thickness was simulated. For the helical cases, a unity pitch was used.

C. Simulated signal-to-noise

Projections consisting of only noise were generated, processed by the various helical methods, and then reconstructed. A region-of-interest was overlayed on top of the image and the standard deviation of the noise was calculated. The results are summarized in Table II with and without dose normalization. Note that the VSH-FS and VSH-US results are identical to the CSH-FS and CSH-US results, respectively.

The following comments are made with respect to the noise measurement for CZA-FS. CSH-FS should be the same because there is no weighting of the projections. CSH-HS shows a large increase because only about half the data is used. When dose is considered, the methods produce comparable results. CSH-US has a slight increase because of the attenuation and amplification of projections. CSH-OS shows a slight reduction because of the overscan region. CSH-HI exhibits a large reduction because twice as much data are used. The reduction is $\sqrt{2/3}$, as theoretically expected, confirming the simulation accuracy. The rest of the results use about 360° of projections and use some projection weighting and therefore should produce slightly higher noise readings. In standard CT scanning, the increased noise of underscan is not noticed. Therefore, CSH-HE, CSH-US, CSH-HH, and VSH-US should also be acceptable from a noise point of view. However, from a straight noise point of view, CSH-HI is the best algorithm.

D. Simulated artifacts

An ellipsoid that was partially protruding into the scan volume centered at the slice plane was simulated. The ellipsoid was 100 mm long in the axial direction and had a 6-mm-diam cross section at its center. It was positioned so that the bottom of the ellipsoid was 5 mm above the slice plane.

The reconstructions for the ellipsoid are shown in Fig. 8. The mean-square-error (MSE) with respect to the CZA-FS case is shown in Table II. The MSE was calculated after deleting the center portion of the images. The deletion was done so that only the streak artifacts were measured and not the differences in the slice profiles.

The test is very severe and probably overestimates the arti-

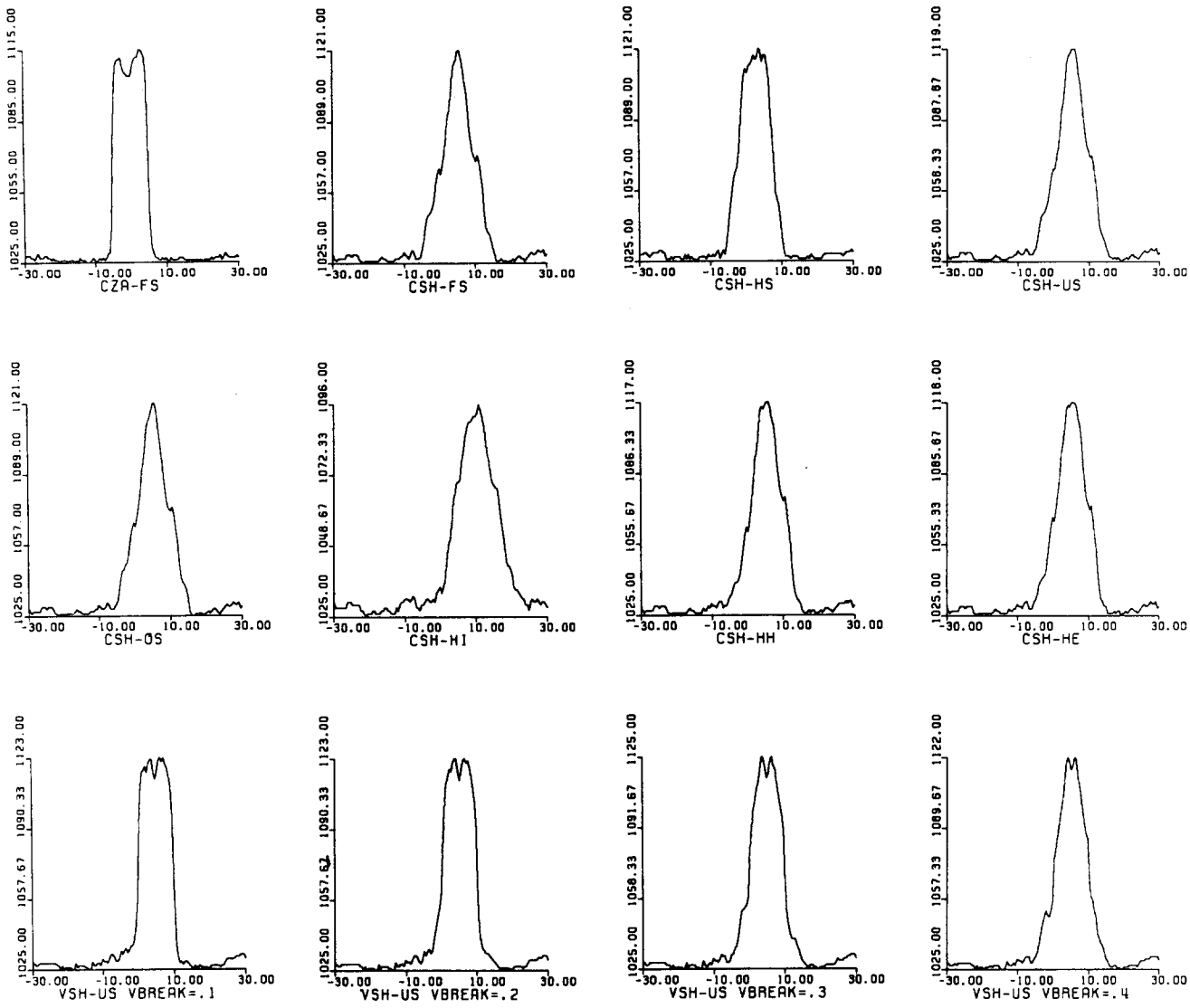

FIG. 7. Maximum-value projections of the images shown in Fig. 6. The units on the horizontal and vertical axes are millimeters and Hounsfield Units (HU), respectively.

facts that would actually be seen in clinical images. Therefore any method beside CSH-FS and CSH-HS would yield acceptable results.

E. Evaluation of the Bresler/Skrabacz algorithm

We implemented the Bresler/Skrabacz algorithm using the coefficients found using Eq. (14) for 1440° of projections using $L = 2$ and α equal to 0.5 and 1.0. The artifacts and the FWHM values are found to be equivalent to CSH-HI for all α.The main problem with their method is that the FWTM for the simulated slice profiles were 36.00 and 39.84 for α equal to 0.5 and 1.0, respectively.We speculate that if 720° of data were used, the FWTM values would still be inferior to CSH-HE. Therefore, we conclude that this algorithm does not offer an improvement over the other algorithms presented here.

IV. EXPERIMENTAL RESULTS

In order to assess the trade-offs posed by the different reconstruction methods, we modified a conventional CT scanner to produce helical data. In this section we discuss the details of this modification and the results of reconstructing the data with the various algorithms.

A. Experimental data collection

We denote a *segment* to be 360° of a helical scan. A segment can be collected using any conventional scanner by translating the table during normal data collection. Because we were not able to easily modify a scanner's software, we chose to drive a table with external sources. For CSH we attached an external displacement unit to a table. In the case

TABLE II. Quantitative results of computer simulations. Shown are full-width-at-half-maximum (FWHM) and full width at tenth-maximum (FWTM) values of the projections shown in Fig. 7; standard deviation, σ, of the simulated noise for different data collection and reconstruction modes with and without dose normalization; and mean-square-error (MSE) of the images shown in Fig. 8 with respect to the CZA case. The MSE was calculated after deleting the center portion of the images so that only the streak artifacts were measured and not the differences in the slice profiles. The units for the standard deviation and the MSE are arbitrary. The notation NA means not applicable. The dose-normalized standard deviation is also normalized by the noise in the CZA-FS case.

Method	*vbreak*	FWHM (mm)	FWTM (mm)	σ	$\frac{\sigma}{\sigma_{\text{CZA-FS}}}\sqrt{\text{Dose}}$	MSE
CZA-FS	NA	10.39	11.34	4.6	1.00	0.00
CSH-FS	NA	7.74	18.13	4.6	1.00	6.79
CSH-HS	NA	9.24	15.24	6.4	1.00	8.33
CSH-US	NA	8.80	17.90	5.0	1.09	1.24
CSH-OS	NA	7.74	18.50	4.5	1.04	3.13
CSH-HI	NA	13.22	19.29	3.8	1.17	0.57
CSH-HH	NA	10.05	17.48	5.3	1.17	0.76
CSH-HE	NA	8.79	17.25	5.3	1.15	0.76
VSH-US	0.1	9.97	11.93	5.0	1.09	0.49
VSH-US	0.2	10.00	13.54	5.0	1.09	1.09
VSH-US	0.3	10.03	16.40	5.0	1.09	1.66
VSH-US	0.4	10.09	17.90	5.0	1.09	1.79

of VSH, we applied an external voltage to the translation motor that is present in a table.

The basis of the unit that was used for CSH is a motor that is mounted on a slider mechanism. The shaft of the motor was attached to a screw. The pitch of the screw and the speed of the motor were chosen to translate the table at 10 or 5 mm/s. The complete unit was set on the end of the table so that the end of the shaft was positioned next to the wall opposite the scanner. When a voltage was applied to the motor, the shaft caused the table to be pushed away from the wall. A microswitch was placed under the sliding portion of the unit. The contacts of the switch were connected to a relay which was wired in parallel with the scan enable button on the operator's console. A scan was begun by setting up the scanner to collect a scan and then to apply a voltage to the motor.The switch was positioned so that, after the motor was running at a constant velocity, it tripped the microswitch which in turn started the scan. Because the scanner starts data collection at a fixed time after depression of the scan enable button, a segment could be repeated. Contiguous segments were collected by displacing the switch by the same amount that the table had to be translated in 360°.

For VSH, the scanner was modified to allow independent control of the table motor using a microcomputer (PC). The PC started the scan by sending a signal to the relay described above. The collimator was selected for the experiment to produce a CZA slice thickness of 10 mm. The table velocity was empirically adjusted, by examining scans of a wire, to give 5 mm of table movement during the beginning of each scan and 5 mm during the end. Several choices of the ramp-up and ramp-down times were examined. In all cases, approximately the same time was used for both ramp-up and ramp-down. Finally based on the computer simulation results, it was decided to use a ramp time of 0.4 s. This corresponds to a value of the variable vbreak of 0.2 since the scan time was 2 s.

The experiments were performed using a GE 9800 Hilight (GE Medical Systems, Milwaukee) scanner in a factory setting. The scanner was maintained so that functionality, but not image quality, could be verified for new software releases. Instead of using the software present in the scanner, we reconstructed projection data with special programs that ran on another computer system. The special programs produced results that were close to clinical 9800 Hilight images but not identical. Therefore the images shown in this section are consistent but cannot be compared to images that would be generated on a similar scanner in a clinical setting.

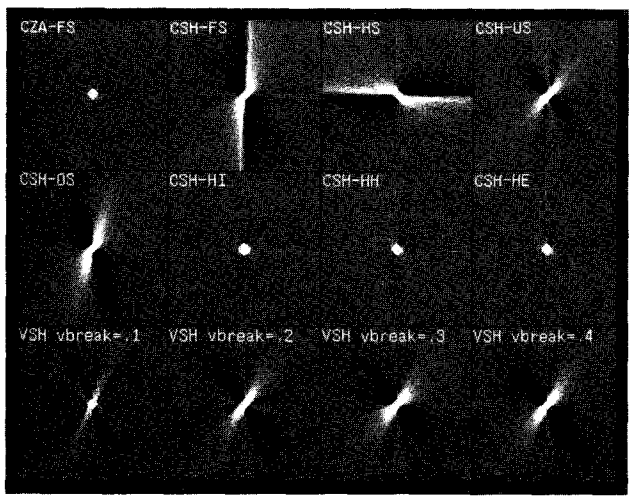

FIG. 8. Simulated reconstructions of an ellipsoid partially protruding into the slice volume for different data collection and reconstruction modes. A 10-mm slice thickness was simulated. For the helical cases, a unity pitch was used.

B.Scanning results

We scanned three healthy volunteers and collected a number of segments for CSH and VSH. Along with the helical images, CZA images at approximately the same slice plane were collected. The time between segments was approximately one minute. Therefore, the subjects had to breathe between the segments. They were given a few seconds warning before the scans were taken in anticipation of arresting their respiration at a consistent point. We had varying degrees of success with this method. In two cases, the volunteers ingested Gastrographin prior to scanning. We scanned using 120 kV, 170 mA, or 200 mA and two second scan times. Almost all of the data were collected using collimation set up to produce CZA data with 10-mm-thick slices. We performed one study in which 5-mm helical data was compared with 5-mm and 10-mm CZA data. (The notation of number preceding a scan type indicates that the collimator is set to produce the specified slice thickness if the table was not translated.) We also experimented with different pitches. Generally, we scanned with a pitch of one. The images were reconstructed using the methods described in Sec.

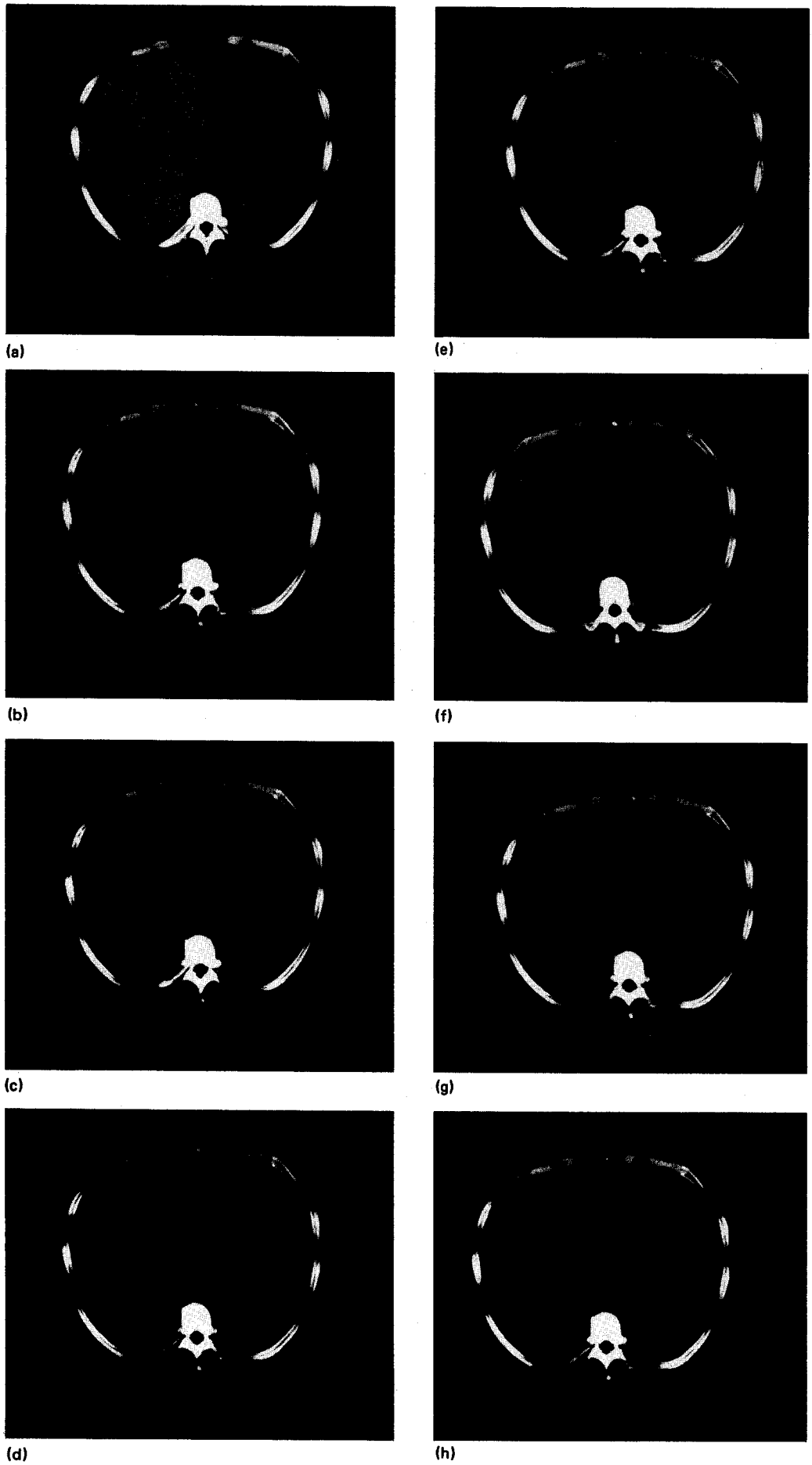

FIG. 9. Reconstructions of experimental data collected from a modified scanner comparing CZA to CSH. The following data collection and reconstruction techniques were employed: (a) CZA-FS, (b) CSH-FS, (c) CSH-HS, (d) CSH-OS, (e) CSH-US, (f) CSH-HI, (g) CSH-HH, and (h) CSH-HE.

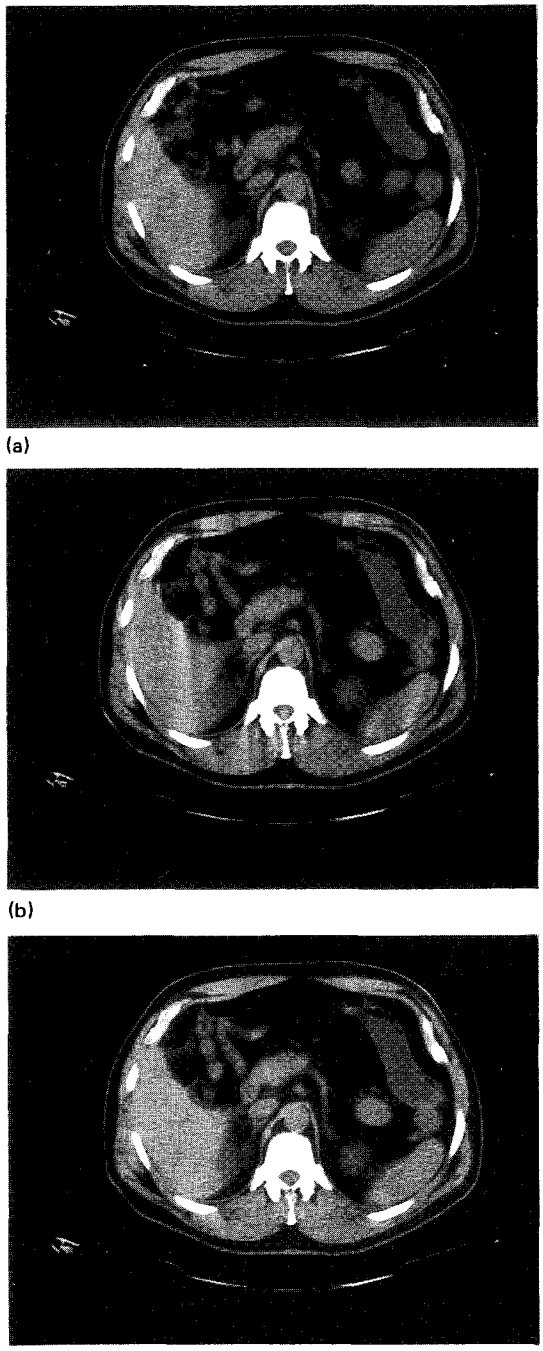

(a)

(b)

(c)

FIG. 10. Reconstructions of experimental data collected from a modified scanner comparing CZA to VSH. The following data collection and reconstruction techniques were employed: (a)CZA-FS, (b) VSH-FS, and (c) VSH-US.

II. We present a complete discussion of the experimental results in the next section. Here we would like to present a few images that are representative of the data that was collected.

Figure 9 shows reconstructions using CZA and CSH for one of the patients where the slice thickness was 10 mm and a pitch of one was used. CSH-FS exhibits broad vertical streaks. The CSH-HS reconstruction demonstrates a change in noise and insufficient view streaks. The CSH-HI case has reduced noise and significant slice profile degradation. CSH-HI and CSH-OS still exhibit more vertical streaking than we expected from the computer simulations. We suspect that the discrepancy is due to respiration being suspended at different locations. In the remaining three cases, CSH-US, CSH-HH, and CSH-HE, the vertical streaks have been eliminated. Varying degrees of slice profile degradation are present in all the CSH results.

Figure 10 shows reconstructions using CZA and VSH for another subject. The collimation was set to produce CZA slices with a 10-mm slice thickness. The VSH-FS reconstruction also shows vertical streaks caused by the inconsistencies in the projection data. The streaks are eliminated in the VSH-US reconstruction. Some slice profile degradation is also present.

V. DISCUSSION

The computer simulations and the experimental results demonstrated that good image quality can be obtained with helical scanning. There is some degradation present in the images. The degradation consists of increased slice thicknesses, a change in noise, and possibly insufficient elimination of structured artifacts. Therefore, helical scanning cannot be used as a direct replacement for CZA assuming that the same collimation is used. In this section we compare the various scanning techniques and reconstruction algorithms and try to determine which method produces images closest to CZA. We also discuss the potential applications of helical scanning.

We begin our discussion with the determination of the best CSH reconstruction algorithm. CSH-FS produces unacceptable results because vertical streaking is not eliminated. CSH-HS produces images with too much noise. CSH-HI removes the streak artifacts and lowers noise, but at the expense of significant slice profile degradation. The remaining algorithms produce similar results with respect to noise and slice profiles. The computer simulations showed that CSH-OS and CSH-US produced more structured artifacts than CSH-HH and CSH-HE. These artifacts are not seen in the experimental results because, we suspect, they are suppressed by quantum noise. The amount of degradation caused by patient motion is proportional to the scan time. Therefore CSH-OS and CSH-HH are less preferable than CSH-US and CSH-HE. We conclude that CSH-US and CSH-HE are the best algorithms. CSH-US might be chosen because it could already be implemented in a scanner.

For values of vbreak less than about 0.2, better results are obtained for VSH than for CSH. VSH is much more difficult to implement because of the requirements placed on moving the table at a variable speed. Also, we suspect that motion artifacts might be introduced with rapid table accelerations. Values of vbreak less than 0.2 might be difficult to implement because of limitations placed on the motor used to drive a table.

Preliminary feedback from radiologists indicates that the helical reconstruction methods remove the structured artifacts that are caused by the simultaneous patient translation

and do not significantly change the signal-to-noise ratio. However, the slice profile degradation was noticed. The helical images were judged to be worse than the CZA image collected at the same slice thickness and better than the CZA image collected at twice the thickness. The difference between VSH and CZA was judged to be smaller than the difference between CSH and CZA. The clinical feedback that we have received so far indicates that the increased partial volume artifacts that arise during helical scanning would be tolerated in exchange for increased scan rate in certain situations. The increased scan rate could be used to enhance the utilization of contrast material for imaging contrast mechanics or to scan a complete organ in a single breath-hold.

An application where helical scanning may be useful is surveying of the chest, abdomen and pelvis. In some cases scan rate is more important than the ultimate contrast detail. Applications may include trauma, pediatric patients and ICU patients. The total scan time is also very critical when the high cost (at least in the U.S.) of nonionic contrast is considered. Another application of helical scanning is in dynamic liver studies. In order to optimize the use of contrast, the liver should be scanned in less than three minutes and under two is optimum.[36] In both cases, helical scanning allows for more slices to be acquired in a single breath-hold. It may be possible to scan the complete liver in a single breath-hold if the patient can hold his/her breath for an extended period of time.[37,38]

The increase in scan rate that might be possible with helical scanning can be demonstrated with the following example. Assume that patients can hold their breath for ten seconds and an IGD of six seconds is required. Also assume that the scan time is one second and the ISD (only the table has to move because of continuous rotation of the gantry) is also one second. Finally, assume that the scan rate is not limited by tube cooling requirements. Then for CZA a group consists of five scans and four ISDs yielding a scan rate of 20 scans/min. Now consider one of the helical methods that utilize 360° of projections. These methods would be CSH-US, CSH-HE or VSH-US. For helical scanning with a unity pitch, a group consists of ten scans and no ISD is required. Therefore, the scan rate for helical scanning is 37.50 scans/min.

We investigated the use of pitches larger than one. The results were more structured artifacts and more degradation of the slice profile. Helical scanning with pitches larger than one could be used in surveying gross anatomy. We also investigated the use of pitches less than one. A problem is that in order to maintain constant dose, the current given to the tube must be reduced or the collimation narrowed. In either case, the tube will not be used efficiently. Another problem with small pitch helical scanning is that it negates the advantage of increased scan rate.

VI. CONCLUSIONS

We have shown that acceptable image quality is obtained in CT reconstructions when the patient is translated concurrently with data acquisition. The patient can be translated at either a constant or variable speed. We presented a number of methods to reconstruct the resulting projection data. Computer simulations and experimental scanning demonstrated that the methods remove the structured artifacts that are present when the simultaneous patient translation is ignored. The results also show that some increase in partial volume artifacts is seen. Review of preliminary results by a panel of radiologists indicates that the residual image degradation is tolerable for selected applications when it is critical to acquire more slices in a patient breathing cycle than is possible with conventional scanning. Additional experiments in a clinical setting are required so that the potential benefits of the helical methods can be better understood.

ACKNOWLEDGMENTS

The authors would like to thank Stan Fox and Jackie Schenck for their helpful discussions on the clinical applications of this work and for supervising the experimental data collection. Albert Lonn read this manuscript and made numerous suggestions relative to the algorithmic aspects of this work. Phil Jones, Gary Sima, David Frazee, and Owen Dake made the modifications required to collect the experimental data. Jim Colsher and Norbert Pelc made numerous comments on the interpolation techniques. Yoram Bresler provided references and software for the Bresler/Skrabacz algorithm. Finally, the authors would like to acknowledge the clinical perspective provided by the following radiologists: Lincoln Berland, Sylvester Chuang, Hugh Curtain, Dennis Foley, David Godwin, Sadek Hilal, Robert Kaufman, Alec Megibow, Peter Selzer, Brook Jeffrey, Reed Dunnick, James Ellis, Elias Kazam, Thomas Lawson, Randolph Ramey and William Shuman.

APPENDIX A: OVERSCAN

In this appendix we review a method that reduces the effect of motion in conventional (CZA) CT scanning. Patient motion artifacts in fullscans are frequently streaks along lines parallel to the rays of the first view. This leads to the observation that motion frequently causes views at the beginning and end of a full scan to be very inconsistent when ideally they should be nearly identical. By contrast, patient motion causes only very small differences from one view to the next. The small view-to-view differences accumulate during a scan to produce a large inconsistency between the first and last views. The small view-to-view differences are not very important, however the large inconsistency is very important. The effect of the data inconsistency is ameliorated[39] by taking extra views at the end of the scan through some angle β_o (the *overscan* angle). This algorithm is called *overscan* and we use the abbreviation OS to denote its use. The extra data in the interval $(2\pi,2\pi+\beta_o)$ are blended in with the data at the beginning of the scan in the interval $(0,\beta_o)$ thus reducing the inconsistency. A weighting function such as

$$w[x(\beta,\gamma)] = 3x^2(\beta,\gamma) - 2x^3(\beta,\gamma), \tag{15}$$

where

$$x(\beta,\gamma)=\begin{cases}\dfrac{\beta}{\beta_0} & 0\leqslant\beta\leqslant\beta_o\\ 1 & \beta_0\leqslant\beta\leqslant 2\pi\\ \dfrac{2\pi+\beta_o-\beta}{\beta_o} & 2\pi\leqslant\beta\leqslant 2\pi+\beta_o\end{cases}\qquad(16)$$

has been found desirable because the derivatives of $w(x)$ with respect to x are zero for $x=0$ and $x=1$. The disadvantages of overscan are that it delivers extra dose and has the potential for even more patient motion than a fullscan. Also, it must be selected prospectively, so that if patient motion is negligible, the extra dose is wasted.

APPENDIX B: UNDERSCAN

The disadvantages of overscan led to the development of a correction method called *underscan* which does not require extra data.[22] We use the abbreviation US for underscan. By underweighting the projection data near the beginning and end of a scan, the inconsistency caused by patient motion can be reduced without collecting extra views. The underweighting is compensated by overweighting projection data acquired near the middle of the scan.

The weighting is constrained by the fact that a fanbeam scan with β in the interval $(0,2\pi)$ contains two samples of each ray. The two redundant sample locations (β_1,γ_1) and (β_2,γ_2) are related by Eq. (12).This requires that the weights $w(\beta,\gamma)$ satisfy

$$w(\beta,\gamma)+w(\beta+\pi+2\gamma,-\gamma)=2.\qquad(17)$$

Suppose, for example, that the weights ramp up from 0 to 1 over some angle β_u (the underscan angle), at the beginning of the scan, and similarly, ramp down from 1 to 0 over the same angle β_u at the end of the scan. Using the weighting function in Eq. (15) for the ramp up and ramp down, for example, and the constraint in Eq. (17), the weights are

$$w(\beta,\gamma)=\begin{cases}3x^2-2x^3 & \text{where } x=\dfrac{\beta}{\beta_u} & 0\leqslant\beta\leqslant\beta_u\\ 1 & & \beta_u\leqslant\beta\leqslant\pi-\beta_u-2\gamma\\ 2-(3x^2-2x^3) & \text{where } x=\dfrac{|\beta-\pi+2\gamma|}{\beta_u} & \pi-\beta_u-2\gamma\leqslant\beta\leqslant\pi+\beta_u-2\gamma\\ 1 & & \pi+\beta_u-2\gamma\leqslant\beta\leqslant 2\pi-\beta_u\\ 3x^2-2x^3 & \text{where } x=\dfrac{2\pi-\beta}{\beta_u} & 2\pi-\beta_u\leqslant\beta\leqslant 2\pi\end{cases}\qquad(18)$$

APPENDIX C: HALFSCAN

Parallel geometry reconstruction requires a minimum data set in which the parallel view angle, $\theta=\beta+\gamma$, spans a range of π. A fanbeam data set with β spanning a range $\pi+2\gamma_m$ contains such a minimum parallel data set. A fanbeam reconstruction algorithm using this data set is called *halfscan* and we use the abbreviation HS to denote its use. Figure 11 shows the Radon space for halfscan. Unfortunately, this fan-beam data contains redundant samples of some of the rays (assuming no patient or table motion). The redundant areas are shaded in Fig. 11. If the redundancy was not eliminated, gross shading in the reconstructed image would result.

The redundant sample locations are related by Eq. (12). The redundancy is eliminated by multiplying the projection data by a set of weights $w(\beta,\gamma)$ which satisfy[21]

$$w(\beta,\gamma)+w(\beta+\pi+2\gamma,-\gamma)=1\qquad(19)$$

such as given, for example, by

$$w[x(\beta,\gamma)]=3x^2(\beta,\gamma)-2x^3(\beta,\gamma),\qquad(20)$$

where

$$x(\beta,\gamma)=\begin{cases}\dfrac{\beta}{2\gamma_m-2\gamma} & 0\leqslant\beta\leqslant 2\gamma_m-2\gamma\\ 1 & 2\gamma_m-2\gamma\leqslant\beta\leqslant\pi-2\gamma\\ \dfrac{\pi+2\gamma_m-\beta}{2\gamma_m+2\gamma} & \pi-2\gamma\leqslant\beta\leqslant\pi+2\gamma_m\end{cases}\qquad(21)$$

The above weights are continuous and differentiable everywhere. Other weights are also possible. For example, the weighting

$$w(\beta,\gamma)=\begin{cases}1 & 0\leqslant\beta\leqslant\pi-2\gamma\\ 0 & \pi-2\gamma<\beta\leqslant\pi+2\gamma_m\end{cases}\qquad(22)$$

eliminates the redundancy. Unfortunately, the weighted projection data would be discontinuous in β and γ along the line $\beta=\pi-2\gamma$. If the projection data were not sampled, no problem would result. However the discontinuity in the discretely sampled projection data would cause severe streaks parallel to rays of the first view. The artifacts can be eliminated by feathering the weights along the discontinuity at $\beta=\pi-2\gamma$ as discussed in Appendix D.

In the latter of the halfscan reconstructions, the smoothed weight is

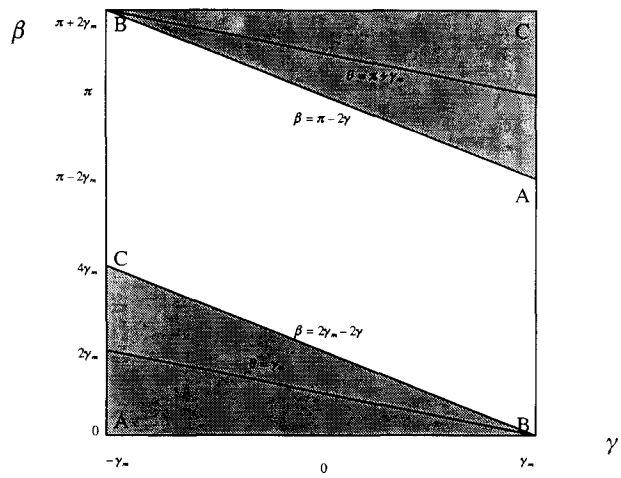

FIG. 11. Radon space for halfscan data collection and reconstruction. The shaded areas contain redundant information.

$$w(\beta,\gamma)=\begin{cases}1 & 0\leqslant\beta\leqslant\pi-2\gamma\\ 1-f\left(\dfrac{\gamma-\gamma_0(\beta)}{d}+\dfrac{1}{2}\right) & \pi-2\gamma<\beta\leqslant\pi+2\gamma_m\end{cases}. \tag{23}$$

where $\gamma_0(\beta)=(\pi-\beta)/2$ and $f(\gamma)$ is defined in Appendix D. A feathering distance d corresponding to 10 detector channels has been found sufficient. The smoothing causes the weights to depart slightly from those ideally required. However we have observed no significant artifact thereby induced. Other weighting schemes are possible, such as weighting the upper and lower shaded triangles in Fig. 11 by 0.5 and the remainder of the data by 1. The above smoothing would be required at the discontinuities.

APPENDIX D: FEATHERING

The feathering algorithm is illustrated by the following example. Suppose $w_1(x)$ and $w_2(x)$ are two functions to be joined at a point $x=x_0$ as follows

$$w(x)=\begin{cases}w_1(x) & x<x_0\\ w_2(x) & x\geqslant x_0\end{cases}, \tag{24}$$

and where $w_1(x_0)\neq w_2(x_0)$ so that $w(x)$ is discontinuous at $x=x_0$. The discontinuity can be smoothed by extending w_1 and w_2 by a distance $d/2$ on either side of $x=x_0$ and weighting them so they blend together over the interval d. This is accomplished by multiplying w_2 by

$$f\left(\frac{x-x_0}{d}+\frac{1}{2}\right), \tag{25}$$

and w_1 by

$$1-f\left(\frac{x-x_0}{d}+\frac{1}{2}\right), \tag{26}$$

and summing, where $f(x)$ is given, for example, by

$$f(x)=\begin{cases}0 & x<0\\ 3x^2-2x^3 & 0\leqslant x\leqslant 1\\ 1 & x>1\end{cases}. \tag{27}$$

[1]R. A. Brooks and G. DiChiro, "Slice geometry in computer assisted tomography," J. Comput. Assist. Tomog. **1**, 191–199 (1977).
[2]P. A. Filipczak, Slip ring assembly for high voltages, U.S. Patent No. 2,979,685 (1961).
[3]K. L. Dinwiddie, R. G. Friday, J. A. Racz, and E. J. Seppi, "Tomographic scanning apparatus having detector signal digitizing means mounted to rotate with detectors," U. S. Patent No. 4,190,772 (1980).
[4]D. L. Parker, J. L. Couch, K. R. Peschmann, V. Smith, M. Jimbo, and E. C. Wang, "Design constraints in computed tomography: a theoretical review," Med. Phys. **9**, 531–539 (1982).
[5]G. Kowalski, "Suppression of ring artifacts in CT fan-beam scanners," IEEE Trans. Nucl. Sci. **NS-25**, 1111–1116 (1978).
[6]D. A. Freundlich, "Ring artifact correction for computerized tomography," U.S. Patent No. 4,670,840 (1987).
[7]P. M. Joseph and R. D. Spital,"A method for correcting bone induced artifacts in computed tomography scanners," J. Comput. Assist. Tomog. **2**, 100–108 (1978).
[8]J. P. Stonestrom, R. E. Alvarez, and A. Macovski, "A framework for spectral artifact corrections in x-ray CT," IEEE Trans. Biomed. Eng. **BME-28**, 128–141 (1981).
[9]P. K. Kijewski and B. E. Bjarngard, "Correction for beam hardening in computed tomography," Med. Phys. **5**, 209–214 (1978).
[10]G. H. Glover and N. J. Pelc, "Nonlinear partial volume artifacts in x-ray computed tomography," Med. Phys. **7**, 238–248 (1980).
[11]G. Henrich, "A simple computational method for reducing streak artifacts in CT images," Comput. Tomog. **4**, 67–71 (1980).
[12]P. M. Joseph and R. D. Spital, "The effects of scatter in x-ray computed tomography," Med. Phys. **9**, 464–472 (1982).
[13]G. H. Glover, "Compton scatter effects in CT reconstructions," Med. Phys. **9**, 860–867 (1982).
[14]J. R. Mayo, N. L. Muller, and R. M. Henkelman, "The double-fissure sign: a motion artifact on thin section CT scans," Radiology **165**, 580–581 (1987).
[15]R. D. Tarver, D. L. Conces, and J. D. Godwin, "Motion artifacts on CT simulate bronchiectasis," Am. J. Roentgenol. **151**, 1117–1119 (1988).
[16]I. Mori, "Computerized tomographic apparatus utilizing a radiation source," U.S. Patent No. 4,630,202 (1986).
[17]H. Nishimura and O. Miyazaki, "CT system for spirally scanning subject on a movable bed synchronized to x-ray tube revolution," U.S. Patent No. 4,789,929 (1988).
[18]W. Kallender, W. Seissler, and P. Vock, "Single-breath-hold spiral volumetric CT by continuous patient translation and scanner rotation," Radiology **173P**, 414 (1989).
[19]P. Vock, H. Jung, and W. Kallender, "Single-breath-hold spiral volumetric CT of the hepatobillary system," Radiology **173P**, 377 (1989).
[20]P. Vock, H. Jung, and W. Kallender,"Single-breath-hold spiral volumetric CT of the lung," Radiology **173P**, 400 (1989).
[21]D. L. Parker, "Optimal short scan convolution reconstruction for fan-beam CT," Med. Phys. **9**, 254–257 (1982).
[22]N. J. Pelc and G. H. Glover, "Method for reducing image artifacts due to projection measurement inconsistencies," U.S. Patent No. 4,580,219 (1986).
[23]A. C. Kak, "Computerized tomography with x-ray, emission and ultrasound sources," Proceedings IEEE **67**, 1245–1272 (1979).
[24]A. C.Kak and M. Slaney, *Principles of computerized tomographic imaging* (IEEE Press, New York, 1987).
[25]J. Namikawa, "Method of collecting data for x-ray tomograph," U.S. Patent No. 4,852,132 (1989).
[26]G. T. Herman, A. V. Lakshminarayanan, A. Naparstak, E. L. Ritman, R. A. Robb, and E. H. Wood, in *Medical Data Processing Symposium* (Taylor and Francis Ltd., London, 1976).
[27]R. N. Bracewell and A. C. Riddle, "Inversion of fan-beam scans in radio astronomy," Astrophs. J. **150**, 427–434 (1967).
[28]C. J. Skrabacz, "Helical scan computerized tomography," MSEE Thesis, University of Illinois, Urbana, IL (1989).
[29]Y. Bresler and C. J. Skrabacz, "Optimal interpolation in helical scan computed tomography," Proc. ICASSP, Vol. 3 1472–1475 (1989).

[30]G. Oetken, T. W. Parks, and H. W. Schussler, "New results in the design of digital interpolators," IEEE Transactions on Acoustics, Speech and Signal Processing **ASSP-23**, 301–309 (1975).
[31]T. W. Parks and D. P. Kolba, "Interpolation minimizing-maximum normalized error for band-limited signals," IEEE Transactions on Acoustics, Speech and Signal Processing **ASSP-26**, 381–384 (1978).
[32]G. Schwierz, W. Lichtenberg, and K. Fuhrer, "Influence of the focal spot on CT image quality," Electromedica **4**, 134–139 (1980).
[33]P. M. Joseph and R. A. Schulz, "View sampling requirements in fan beam computed tomography," Med. Phys. **7**, 692–702 (1980).
[34]R. A. Brooks, G. H. Glover, A. J. Talbert, R. L Eisner, and F. A. DiBianca, "Aliasing: a source of streaks in computed tomograms," J. Comput. Assist. Tomog. **3**, 511–518 (1979).
[35]C. R. Crawford and A. C. Kak, "Aliasing artifacts in computerized tomography," Appl. Opt. **18**, 3704–3711 (1979).
[36]L. L. Berland, *Practical CT technology and techniques* (Raven Press, New York, 1987).
[37]K. Shaffer and R. D. Pugatch, "Small pulmonary nodules: dynamic CT with single-breath technique," Radiology **173**, 567–568 (1989).
[38]N. Sadatoh, H. Hatabu, M. Takahashi, K. Imanaka, and A. Sano, "Oxygen-assisted breath-holding in computed tomography," J. Comp. Assist. Tomog. **11**, 742–744 (1987).
[39]D. L. Parker, V. Smith, and J. H. Stanley, "Dose minimization in computed tomography overscanning," Med. Phys. **8**, 706–711 (1981).